



Fully digital intensity modulated LIDAR

Fabio POLLASTRONE ^{a,*}, Gian Carlo CARDARILLI ^b, Roberto PIZZOFERRATO ^c, Marco RE ^b

^a Department FSN, FUSTEC – IEE - ENEA Frascati, Roma, Italy

^b Department of Electronics Engineering, University of Rome “Tor Vergata”, Roma, Italy

^c Department of Industrial Engineering, University of Rome “Tor Vergata”, Roma, Italy

Received 20 November 2015; revised 17 March 2016; accepted 13 April 2016

Available online 28 April 2016

Abstract

In several applications, such as collision avoidance, it is necessary to have a system able to rapidly detect the simultaneous presence of different obstacles. In general, these applications do not require high resolution performance, but it is necessary to assure high system reliability also within critical scenarios, as in the case of partially transparent atmosphere or environment in presence of multiple objects (implying multiple echoes having different delay times.) This paper describes the algorithm, the architecture and the implementation of a digital Light Detection and Ranging (LIDAR) system based on a chirped optical carrier. This technique provides some advantages compared to the pulsed approach, primarily the reduction of the peak power of the laser. In the proposed architecture all the algorithms for signal processing are implemented using digital hardware. In this way, some specific advantages are obtained: improved detection performance (larger dynamics, range and resolution), capability of detecting multiple obstacles having different echoes amplitude, reduction of the noise effects, reduction of the costs, size and weight of the resulting equipment. The improvement provided by this fully digital solution is potentially useful in different applications such as: collision avoidance systems, 3D mapping of environments and, in general, remote sensing systems which need wide distance and dynamics.

© 2016 China Ordnance Society. Production and hosting by Elsevier B.V. All rights reserved.

Keywords: CW-IM LIDAR; Chirp; Laser Obstacle Avoidance

1. Introduction

LIDAR based on laser beam scanning can be applied to several detection and ranging fields, including obstacle avoidance in aerospace navigation [1] as well as real-time surveillance of restricted areas. For example, LIDAR can be used in port areas security to detect crafts in rapid approach, which are not easily revealed by passive optical systems at night, also considering that RF Radar systems can fail in case of non-conductive or small boats.

Many laser modulation techniques can be applied, obtaining different measurement ranges and resolutions:

- 1) Continuous wave amplitude modulated [2], based on the sinusoidal modulation of the laser beam intensity (sub-millimetrical resolution, single echo and small distance);
- 2) Pulsed LIDAR [3] (long distance, multiple echoes);
- 3) Pulse compression [4,5] (long distance and multiple echoes)

- 4) Continuous wave frequency modulated (CW-FM) technique (long distance and multiple echoes) [6,7].
- 5) Continuous wave intensity modulated [8], based on the laser beam intensity modulated by a chirped signal.

The CW-IM-technique is generally implemented by using analog electronic circuits or optical system. Despite its greater operative frequency which can allow a higher resolution, the use of an analog implementation reduces the flexibility and the robustness of the obtained equipment, and does not enable the application of powerful processing techniques that can improve the performance in presence of multiple echoes with very different amplitudes. On the contrary, a digital approach is able to exploit these techniques, increases the integration and reduces the complexity of the assembling [9]. As a consequence, the resulting devices have reduced costs and increased reliability.

For these reasons during the last years, the authors developed different versions of a fully digital processing system for LIDAR. This system is able to measure the times of flight of the optical wave also in presence of multiple echoes. The system has been developed in a collaboration between ENEA and University of Rome “Tor Vergata”.

Peer review under responsibility of China Ordnance Society.

* Corresponding author. Tel.: +39 06 9400 5535.

E-mail address: fabio.pollastrone@enea.it (F. POLLASTRONE).

All the above versions of the electronic circuits for the LIDAR have been designed and tested; one of these has also been actually applied to an optical laser probe.

This paper describes the CW-IM algorithm used in the experimental equipment, the architecture of the hardware and firmware developed, the test performed and their results.

The paper is organized as follows: in Section 2 the algorithm is briefly discussed, while in Section 3 the architecture of the fast prototype is illustrated. Section 4 contains a discussion on the digital implementation of the proposed algorithm. Section 5 describes the experimental results of a first version of the LIDAR electronic system, while Section 6 contains the preliminary electrical test of the second release. The last section contains the conclusions and the possible future activities.

2. CW-IM algorithm

CW-IM LIDAR technique is based on linear complex chirp signal

$$R(t) = e^{i(2\pi f_r \cdot t)} = R_I(t) + iR_Q(t)$$

where $f_r = \Delta freq/T$ is the increasing rate of chirp frequency, T is the sweep duration and $\Delta freq = stop_freq - start_freq$ is the chirp bandwidth.

The laser beam is modulated with the component

$$R_Q(t) = \sin[(2\pi f_r \cdot t) \cdot t]$$

The echo signal $S(t)$ at the output of the photodiode that receives the lights backscattered from the targets is given by

$$S(t) = A_R \cdot R_Q(t - \Delta t) = A_R \cdot \sin[2\pi f_r (t - \Delta t) \cdot (t - \Delta t)]$$

$S(t)$ corresponds to $R_Q(t)$ delayed by time of flight $\Delta t = 2 \cdot D/C$ (where D is the target distance and C is the speed of light). The amplitude of the echo A_R depends on the target material, the angle of incidence and the distance.

For sake of simplicity, in this discussion additional phase shifts in the echo have not been considered; this assumption does not affect the final results.

The product $C(t) = R(t) \cdot S(t)$ can be expressed as

$$C(t) = C_I(t) + iC_Q(t) = C_{IL}(t) + C_{IH}(t) + iC_{QL}(t) + iC_{QH}(t)$$

where

$$C_{IH}(t) = \frac{1}{2} A_R \sin(4\pi f_r t^2 + 2\pi f_r \Delta t^2 - 4\pi f_r \Delta t \cdot t)$$

$$C_{IL}(t) = \frac{1}{2} A_R \sin(2\pi f_r \Delta t^2 - 4\pi f_r \Delta t \cdot t)$$

$$C_{QH}(t) = -\frac{1}{2} A_R \cos(4\pi f_r t^2 + 2\pi f_r \Delta t^2 - 4\pi f_r \Delta t \cdot t)$$

$$C_{QL}(t) = -\frac{1}{2} A_R \cos(-2\pi f_r \Delta t^2 + 4\pi f_r \Delta t \cdot t)$$

The high-frequency terms C_{IH} and C_{QH} are 2 chirps with double chirp rate and different start and stop frequency with respect to $R(t)$. The most of C_{IH} and C_{QH} signals are removed from the $C(t)$ signal using a complex low-pass filter, as shown in Fig. 1. The remaining low-frequency terms C_{IL} and C_{QL} are

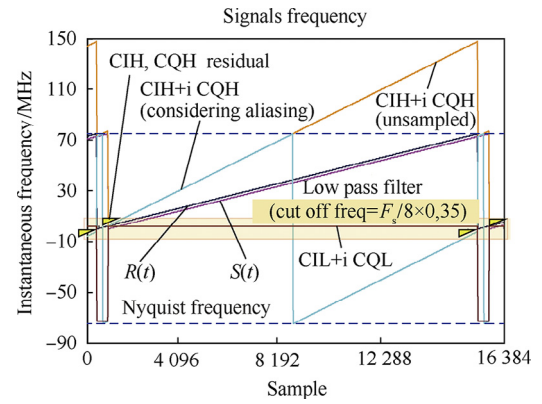


Fig. 1. Trend of the signals frequencies during the chirp period.

2 sinusoids at frequency $2f_r \Delta t$, they depend on the time of flight Δt .

The instantaneous frequencies of the previously described signals are shown in Fig. 1.

In case of multiple echoes with different delays Δt_i , it is possible to know the amplitude A_{R_i} of the single echo by analyzing the module of the Fast Fourier Transform ($/FFT$) of the $(C_{IL} + i C_{QL})$ signal.

3. Architecture of the fast prototyping system

Two fully digital CW-IM LIDAR electronics have been developed starting from Field Programmable Gate Array (FPGA) fast prototyping system [10].

The first release (see Fig. 2) is based on Stratix II EP2S60 DSP Development Board presenting the following characteristics:

- 1) Altera Stratix II EP2S60F1020C4 FPGA;
- 2) 100 MHz system clock;
- 3) Two 12-bit 125 Msps A/D (model AD9433BSQ) converters used in interleaved mode to obtain a 150 Msps analog to digital conversion;
- 4) 14 bit 165 Msps D/A converter (model TI DAC904);
- 5) An Ethernet MAC/PHY;
- 6) A JTAG interface.

Moreover, the hardware contains a signal conditioning circuitry and an optical interface composed by a laser diode and a photoreceiver.

4. Implementation of CW-IM LIDAR algorithm on digital hardware

The proposed algorithm has been implemented through the digital processing of the signals; the main limitations are due to the sampling frequency (F_s) of the A/D converter. If compared with the conventional analog implementations we obtain the following advantages:

- 1) Simplification of the system and lower cost due to the absence of critical analog parts;
- 2) The digital generation of the quadrature complex chirp signal (with frequency in the range $0 - F_s/2$) corresponds to

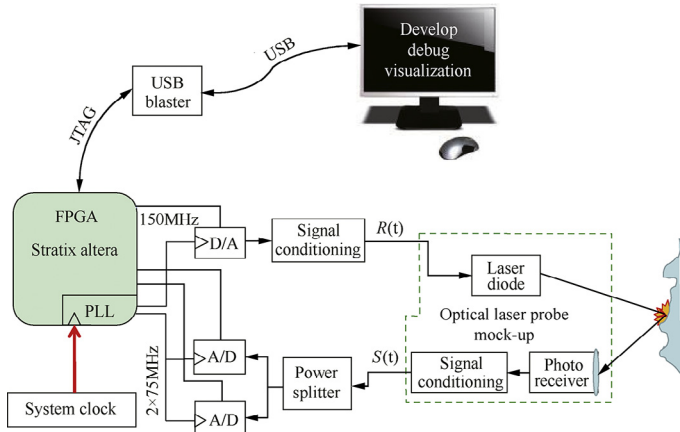


Fig. 2. First version of the fully digital CW-IM LIDAR electronic system. Fast prototyping board architecture.

a better stability/linearity and flexibility in comparison with the analog implementations;

- 3) High linearity of the complex product and of the digital low pass band filters (FIR);
- 4) Small size and very low weight;
- 5) Flexibility due to the possibility to reprogram the FPGA (also in real time) by loading new algorithms;
- 6) Scalability, with the proposed approach we can take full advantage of the technological developments; for example A/D speed improvements can be exploited to increase the resolution;
- 7) The digital implementation inside the FPGA of the complex chirp $R(t)$ makes it possible to use a reference

signal that can be used directly without any A/D conversions. This characteristic permits to use greater word-lengths for the chirp representation, allowing a significant optimization of the algorithm.

The first implementation uses two A/D converters in interleaving mode for increasing the input sampling frequency (up to 150 Msp/s). The performance degradation due to sampling jitter and linearity mismatches of the two A/D converters are acceptable in our application. However, methods for correcting these errors are already present in the literature.

The LIDAR electronic hardware / firmware architecture is shown in Fig. 3. The firmware has been implemented in VHDL by using ALTERA Quartus II Macrofunctions.

The FPGA firmware is composed of the following blocks:

- 1) The inter leaving mux that alternatively selects the S1 and S2 signal, outputting the $S(t)$ echo signal @ 150 Msp/s;
- 2) One *Quadrature Chirp Generator* that generates the $R(t)$ reference modulation chirp (20 bit resolution). The *Quadrature Chirp Generator* is composed of a Numerically Controlled Oscillator (NCO) combined with a *Ramp_generator*. The *Ramp_generator* outputs the *Phase_Increment* (proportional to the instantaneous frequency) and the *Reset* of the NCO and is controlled by the *Chirp_Synch*. The *Chirp_Synch* generates the *Start_Ch* and *Stop_Ch* signals that command the increase and the reset for the *Ramp_Generator*;
- 3) A *Complex Multiplier* implementing the product of the echo signal $S(t)$ and the complex modulation signal $R(t)$;
- 4) A low pass decimator FIR filter implemented by using the Altera FIR compiler tool;

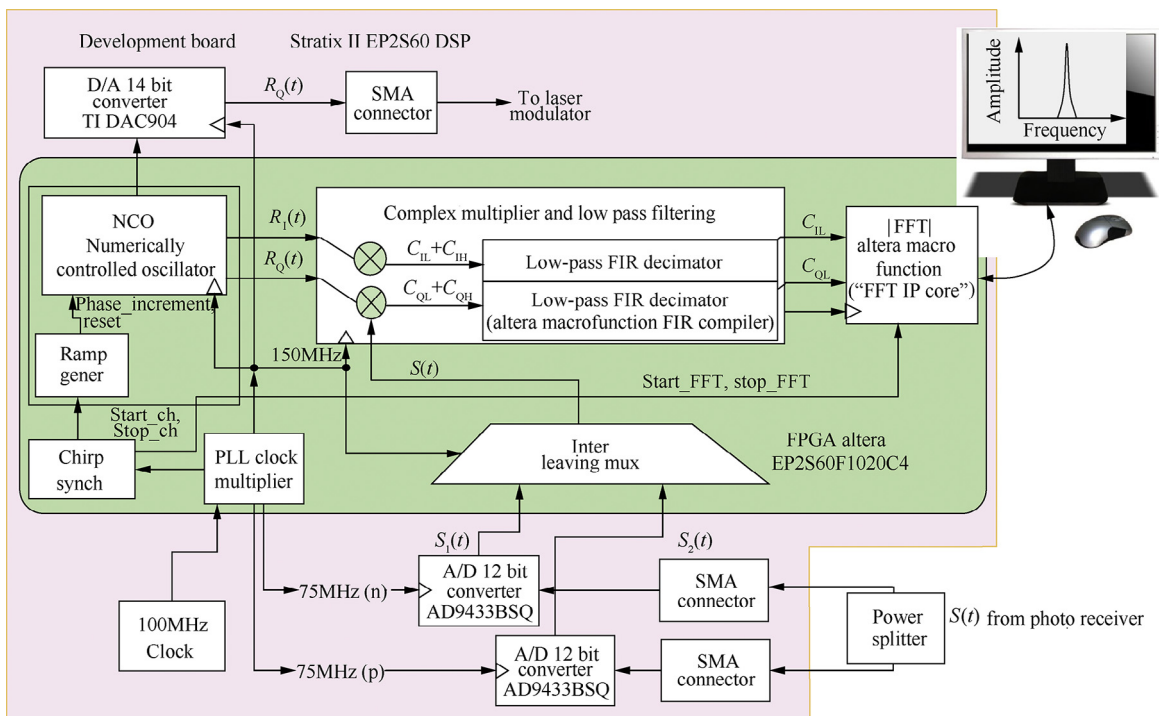


Fig. 3. Hardware / firmware for implementation of the algorithm.

the low pass decimator FIR is composed of two decimator FIR in cascade and the FIR characteristics are reported as the following:

First FIR	
Sampling frequency (F_{s1})	150 MHz
Decimation-factor	4
Taps	50
Window type	Hamming
–3 dB frequency	$F_{s1} \times 0.04$
–55 dB frequency	$F_{s1} \times 0.1$
Second FIR	
Sampling frequency (F_{s2})	$F_{s1}/4 = 37.5$ MHz
Decimation factor	2
Taps	60
Window type	Blackman
–3 dB frequency	$F_{s2} \times 0.1$
–60 dB frequency	$F_{s2} \times 0.18 = 6.75$ MHz

- 5) A floating point FFT (2048 samples), synchronized with the $R(t)$ chirp modulation start, implemented by using the Altera FFT IP Core.

A PC, connected as shown in Fig. 2, is used to configure the FPGA board and to acquire the elaborated signals (such as the FFT result). The connection PC-FPGA board is realized by using the USB blaster device and the Altera software tools.

In the following, some considerations about the frequency limitations related to the digital implementation of the detection algorithm are reported. As shown in Fig. 1 (see curve $R(t)$), it is possible to generate and sample signals with instantaneous frequency up to $F_s/2 = 75$ MHz. Moreover, aliasing phenomena are possible in the high frequency components C_{IH} and C_{QH} of the product signal $C(t)$.

The LIDAR resolution can be improved by increasing the sweep bandwidth and the chirp rate f_i . For this reason and considering the hardware constraint, in the first version of the LIDAR electronic realization the frequency of $R(t)$ has been swept from 0 MHz to 75 MHz. The low pass FIR decimator (*decimation factor* = 8; cut-off frequency $0.35 \cdot F_s/8 < 1/2 \cdot F_s / \text{decimation_factor}$) is needed to remove most of the C_{IH} and C_{QH} components. However, being C_{IH} and C_{QH} two chirp signals, during the chirp period there are two short time intervals where residual signal are present, not removed by the filters (see yellow triangles in Fig. 1). The reduction of the FIR cut-off frequency decreases the duration of C_{IH} and C_{QH} residuals, improving the signal to noise ratio (SNR), but on the other hand reduces the maximum measurable range.

Taking into account the decimation factor and to avoid discontinuity of the C_L components (due to an FFT window longer than the $R(t)$, with the resulting presence of two or more sequences $R(t)$ in the window) the number of samples for the FFT window is limited to 2048. The chirp laser modulation period has been set to 16,384 samples (corresponding to 109 μ s). The characteristics of the used electronic board limit the resolution, because it depends on many parameters (*start_freq*, *stop_freq*, sampling frequency F_s etc.). In our first implementation setting the *start_freq* = 0 and *stop_freq* = $F_s/2$ we obtain

$$\text{resolution} = \frac{\Delta D}{\Delta \text{beam}} = \frac{C}{F_s} = 2 \text{ meters}$$

Table 1

Main parameters related to first fully digital LIDAR electronic developed.

First LIDAR electronic version (main characteristics summary)		FPGA Altera 2S60
A/D	12 bit	
D/A	14 bit	
Chirp generation	Start frequency	0 MHz
	Stop frequency	$F_s/2 = 75$ MHz
Decimator FIR	Cut-off frequency	$(F_s/2) \times (0.35/8)$
	Decimation factor	8
Range	Distance resolution	2 meters
	Max theoretical range	1433 meters
Sweep_duration \equiv measurement time		109 μ s

On the other hand, it is possible to extend the measurement range by increasing the *sweep_duration* or reducing the *decimation_factor*, or by using a more sophisticated laser modulation based on phase-shift keying [11]. The maximum detectable frequency is limited by the cut-off frequency of the FIR decimation filter; in our case, $F_s \times 0.35 / (\text{decimation_factor} \times 0.5)$ is the available output bandwidth. As a consequence, the theoretical range obtained in the developed system is

$$\text{range} = \frac{C \cdot \text{sweep_time}}{2 \cdot \text{decimation_factor}} \cdot \frac{0.35}{0.5} \cong 1433 \text{ meters}$$

Table 1 summarizes the main parameters related to the first version of the Fully Digital LIDAR system.

The measurement throughput ($\cong 10$ kHz) allows low frame rate imaging.

Table 2 reports the Main firmware functions of the CW-IM algorithm. In particular the resource utilization is related to the first version of the LIDAR electronics (FPGA Altera 2S60).

5. System test

The system has been tested by using two different approaches: a) by emulating the optical delay with an electrical delay line; b) by using a laboratory optical set up. Moreover, the experimental results (reported below) were compared and found in agreement with preliminary simulation using Matlab and Simulink,

5.1. Electrical test

An electrical test has been performed on the first version of the LIDAR electronics in order to verify its behavior in the case

Table 2

Main firmware functions and relative utilization of the FPGA resources (first LIDAR electronics Altera 2S60).

Main firmware functions	Adaptive look-up tables	Dedicated logic register	Memory bits	DSP block (9 bit)
NCO	202	456	15,360	32
Complex multiplier	0	0	0	2x8
Fir dec 4 x 2	2,199	4,420	2,048	16
FFT	10,098	13,080	311,552	0
Entire project including	17,457	24,659	1,088,768	84
Signal-tap feature	36%	51%	43%	29%

of various types of signals in input to the system. In particular, the electrical characterization of the digital LIDAR system considers different attenuation and delay times for the echo signal.

The experimental set up is composed of a coaxial cable in series with a variable attenuator that sends back the output of the modulation signal $R_Q(t)$ to the input $S(t)$ signal (Fig. 4). Moreover, a FIFO has been implemented in the FPGA for emulating greater echo delays.

The test carried out on this first version of the LIDAR electronic prototype demonstrates the correctness of the time delay measured, and the linearity of the echo amplitude.

In particular, as shown in Figs. 5 and 6 it is possible to detect echoes with attenuation up to 72 dB, although in this first embodiment it is not possible to discriminate echoes of very

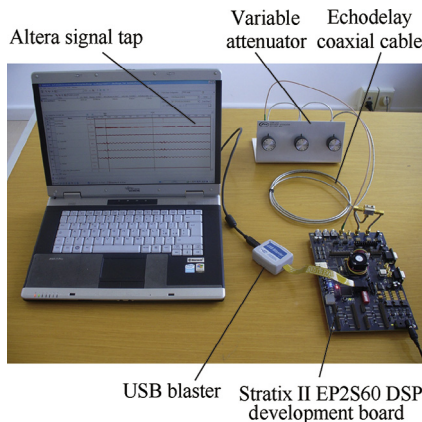


Fig. 4. Electrical test layout for the first LIDAR electronic prototype.

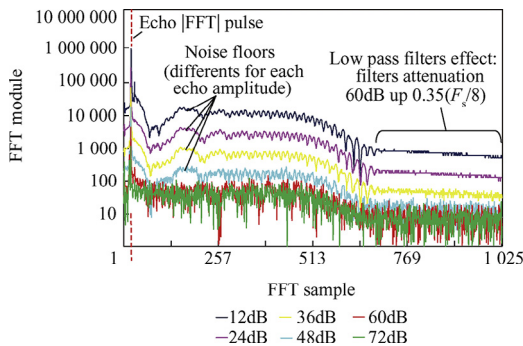


Fig. 5. Electrical tests of the first LIDAR electronic prototype. |FFT| for different echo attenuation.

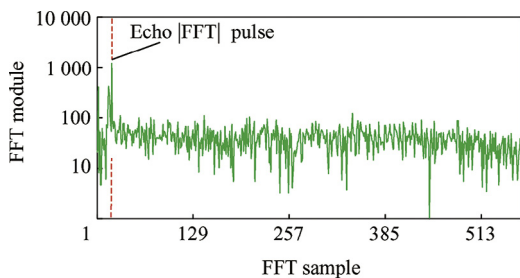


Fig. 6. Distance measure obtained with echo signal attenuated by 72 dB.

different amplitudes. This is due to the fact that the greater echo, through its residues, introduces a background noise that covers the smaller echo. This problem has been reduced in the second LIDAR electronic (see Section 6).

The target distance is calculated applying the equation:

$$echo_distance = dist_offset + resolution \cdot \#sample |FFT|_{peak}$$

where $\#sample |FFT|_{peak}$ represents the bin number (FFT output sample) having the maximum FFT magnitude. The constant $dist_offset$ is due to the hardware component delays (LIDAR electronics, laser, photodetector, cables etc.).

5.2. Optical test

A more sophisticated test bed has been developed by including a simplified Optical Laser Probe, in order to test the above implementation.

In this case the electrical signal $R_Q(t)$ has been connected to the modulation input of a 75 mW CW 660 nm semiconductor laser diode (Melles Griot Mod. 56RCS008/HS), and $S(t)$ is obtained from the electrical output of a photodiode (Thorlabs Mod. PDA10A-EC) with an optical bandwidth from 200 nm to

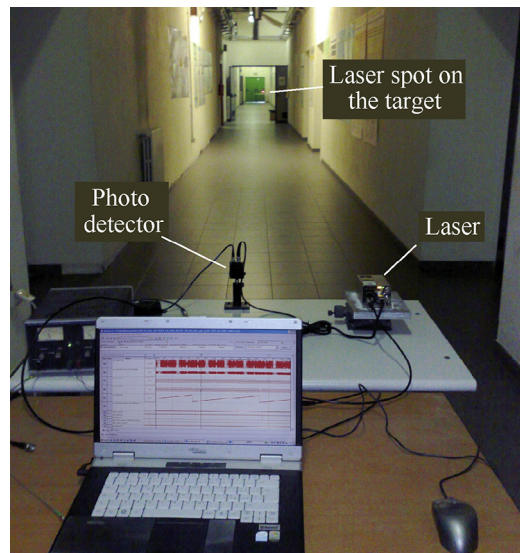


Fig. 7. Photograph taken during optical tests.

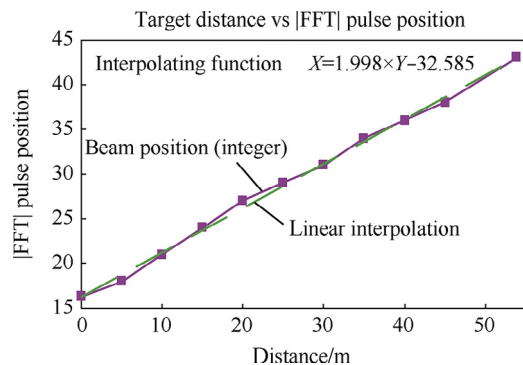


Fig. 8. Optically-measured |FFT| echo distance versus actual target distance.

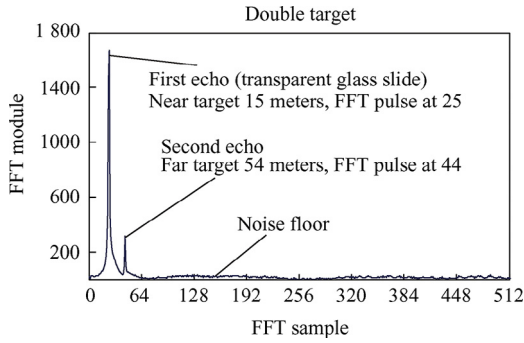


Fig. 9. Optically-measured FFT Module in a double echo case.

1000 nm and a RF output bandwidth from DC to 150 MHz. The experimental set-up is shown in the picture of Fig. 7.

Fig. 8 shows the relation between the measured positions of the obstacle (using FFT magnitude) and the actual target distance; the linearity error is very low in comparison with the theoretical resolution (2 meters).

Fig. 9 shows the output of FFT in the case of presence of two different echoes, the first (15 meters) is related to a transparent glass slide and the second is related to the target (54 meters). Both pulses are easily detectable.

6. Upgrade of the LIDAR electronics end relative tests

The CW-IM digital LIDAR electronics has been recently upgraded to a new version with a more performant proto board. It is based on:

- Altera Stratix 3SL150 FPGA (142K logic elements)
- two 14 bit 150 MSPS A/D converters
- two 14 bit 250 MSPS D/A converters

Considering the increase of the sampling frequency of the A/D converters (overclocked to 165 Msps), the new architecture does not need the interleaving features. Moreover, while the 2 meter distance resolution has been conserved, minor improvements in the algorithm implementation (*start_freq*, *stop_freq*, *sweep_duration*) have been made. In particular, by increasing the out-of-band rejection of the low-pass FIR and the *start_freq*, and reducing the *stop_freq*, the C_H residuals have been drastically reduced.

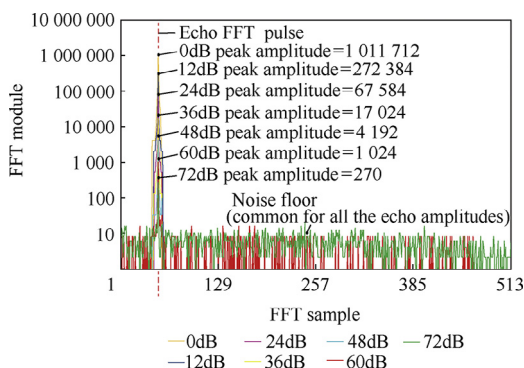


Fig. 10. Electrical tests of the second LIDAR electronic prototype: spectrum vs echo attenuation.

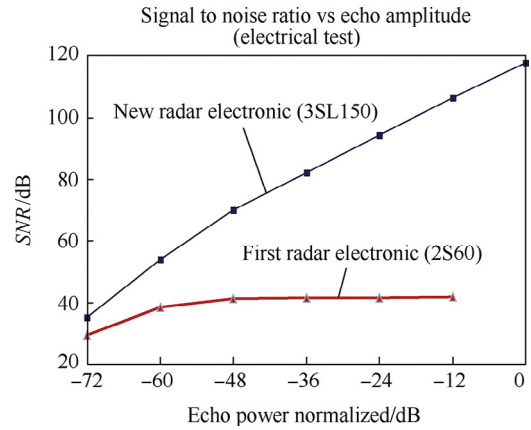


Fig. 11. Electrical test: comparison of the SNR obtained using first and new hardware architecture.

The result is a decrease of the signal noise floor (see Fig. 10) and a consequent improvement of the Signal to Noise Ratio (SNR), particularly in the case of high level echo signals (see Fig. 11). The reduction of the noise level increases the ability to detect small amplitudes echoes, while the increase of SNR allows the detection of simultaneous electrical echoes having very different amplitudes.

Fig. 11 shows the comparison of the SNR between the first and the new version of the LIDAR electronics. On the graph the SNR is represented in relation to the normalized echo input amplitude.

In the first version of the LIDAR electronic system the SNR saturates at about 43 dB, while in the new system the SNR increases fairly linearly with the echo amplitude from 35 dB (in the case of input attenuation of 72 dB) up to 117 dB in the case of full scale echo (0 dB attenuation).

7. Conclusions

In this paper the digital implementation of a LIDAR based on a CW-IM laser modulation has been presented. If compared with the analog implementation, this approach gives interesting advantages in terms of cost, performance, flexibility and physical size of the final equipment. The proposed architecture is based on the FFT which allows a very efficient implementation of the algorithm. The relation between the different algorithm parameters and the system performance has been analyzed. Moreover, the algorithm has been tested implementing two hardware prototypes. These prototypes have been used for different experiments enabling the evaluation of the performance of the whole equipment. All the results show that this technique is suitable to implement an efficient low-cost LIDAR, particularly useful for defense and security applications. The improvements obtained in the second version of LIDAR electronic prototype are particularly interesting in terms of decrease of RNR. Optical tests of the second LIDAR electronic version, connected to the optical laser probe mock-up, are planned. If the improvement of the SNR will be confirmed, the LIDAR prototype will be able to recognize multiples echoes having large difference in amplitudes.

References

- [1] Sabatini R, Richardson MA, Roviato E. Development and flight test of an avionics lidar for helicopter and UAV low-level flight. *J Aeronaut Aerosp Eng* 2013;2:114. doi:10.4172/2168-9792.1000114.
- [2] Pollastrone F, Neri C. Test results for triple-modulation radar electronics with improved range disambiguation. *Fusion Eng Des* 2015;96–97:912–16. doi:10.1016/j.fusengdes.2015.04.056. ISSN 0920-3796.
- [3] Spinhirne JD. Micro pulse lidar. *IEEE Trans Geosci Remote Sens* 1993;31(1):48–55. doi:10.1109/36.210443.
- [4] Allen C, Gogineni S. A fiber-optic-based 1550-nm laser radar altimeter with RF pulse compression. In: *Geoscience and Remote Sensing Symposium, 1999. IGARSS '99 Proceedings. IEEE 1999 International*, vol. 3. 1999. p. 1740–2, doi:10.1109/IGARSS.1999.772080.
- [5] Allen C, Cobanoglu Y, Chong SK, Gogineni S. Performance of a 1319 nm laser radar using RF pulse compression. In: *Geoscience and Remote Sensing Symposium, 2001. IGARSS '01. IEEE 2001 International*, vol. 3. 2001. p. 997–9, doi:10.1109/IGARSS.2001.976726.
- [6] Gao S, Hui R. Frequency-modulated continuous-wave lidar using I/Q modulator for simplified heterodyne detection. *Opt Lett* 2012;37:2022–4. doi:10.1364/OL.37.002022.
- [7] Agishev R, Gross B, Moshary F, Gilerson A, Ahmed S. Range-resolved pulsed and CWFM lidars: potential capabilities comparison. *Appl Phys B* 2006;85:149–62. doi:10.1007/s00340-006-2254-6.
- [8] Campbell JF, Lin B, Nehrir AR, Harrison FW, Obland MD. Super-resolution technique for CW lidar using Fourier transform reordering and Richardson–Lucy deconvolution December 15, 2014 / Vol. 39, No. 24 / OPTICS LETTERS 6981.
- [9] Cardarilli GC, Del Re A, Nannarelli A, Re M. Residue number system reconfigurable datapath, *Proc. IEEE International Symposium on Circuits and Systems, ISCAS 2002, II-756 - II-759 vol.2, 2002*, doi:10.1109/ISCAS.2002.1011463.
- [10] Hamblen JO, Hall TS, Michael D. *Rapid prototyping of digital systems*. SOPC Edition Springer Science; 2008.
- [11] Campbell JF, Lin B, Nehrir AR. Advanced sine wave modulation of continuous wave laser system for atmospheric CO₂ differential absorption measurements. *Appl Opt* 2014;53(5). doi:10.1364/AO.53.000816.